Monthly Notices of the ROYAL ASTRONOMICAL SOCIETY
MNRAS **523,** 2209–2218 (2023) https://doi.org/10.1093/mnras/stad1380

On the growth of supermassive black holes formed from the gravitational collapse of fermionic dark matter cores

C. R. Argüelles,[1,2,3]★ K. Boshkayev,[4,5] A. Krut,[2] G. Nurbakhyt,[4] J. A. Rueda,[2,3,6,7,8]★ R. Ruffini,[2,3,9] J. D. Uribe-Suárez[2,10] and R. Yunis[2]

[1]*Instituto de Astrofísica de La Plata, UNLP-CONICET, Paseo del Bosque s/n B1900FWA La Plata, Argentina*
[2]*ICRANet, Piazza della Repubblica 10, I-65122 Pescara, Italy*
[3]*ICRA, Dipartimento di Fisica, Sapienza Università di Roma, Piazzale Aldo Moro 5, I-00185 Roma, Italy*
[4]*NNLOT, Department of Theoretical and Nuclear Physics, Al-Farabi Kazakh National University, Almaty 050040, Kazakhstan*
[5]*International University of Information Technology, Manas St. 34/1, 050040 Almaty, Kazakhstan.*
[6]*ICRANet-Ferrara, Dipartimento di Fisica e Scienze della Terra, Università degli Studi di Ferrara, Via Saragat 1, I-44122 Ferrara, Italy*
[7]*Dipartimento di Fisica e Scienze della Terra, Università degli Studi di Ferrara, Via Saragat 1, I-44122 Ferrara, Italy*
[8]*INAF, Istituto di Astrofisica e Planetologia Spaziali, Via Fosso del Cavaliere 100, I-00133 Rome, Italy*
[9]*INAF, Viale del Parco Mellini 84, I-00136 Rome, Italy*
[10]*Facultad de Ciencias Básicas, Universidad Santiago de Cali, Campus Pampalinda, Calle 5 No. 6200, 760035 Santiago de Cali, Colombia*

Accepted 2023 May 3. Received 2023 May 3; in original form 2023 February 2

ABSTRACT

Observations support the idea that supermassive black holes (SMBHs) power the emission at the centre of active galaxies. However, contrary to stellar-mass BHs, there is a poor understanding of their origin and physical formation channel. In this article, we propose a new process of SMBH formation in the early Universe that is not associated with baryonic matter (massive stars) or primordial cosmology. In this novel approach, SMBH seeds originate from the gravitational collapse of fermionic dense dark matter (DM) cores that arise at the centre of DM haloes as they form. We show that such a DM formation channel can occur before star formation, leading to heavier BH seeds than standard baryonic channels. The SMBH seeds subsequently grow by accretion. We compute the evolution of the mass and angular momentum of the BH using a geodesic general relativistic disc accretion model. We show that these SMBH seeds grow to $\sim 10^9$–10^{10} $M_\odot$ in the first Gyr of the lifetime of the Universe without invoking unrealistic (or fine-tuned) accretion rates.

Key words: galaxies: formation – galaxies: high-redshift – galaxies: nuclei – quasars: supermassive black holes – galaxies: structure – dark matter.

1 INTRODUCTION

The formation, growth, and nature of the supermassive BHs (SMBHs) residing at the galaxy centres are outstanding problems in astrophysics and cosmology. Important unresolved questions include how can they grow so large and so fast to be present in the farthest distant quasars (Volonteri 2012; Woods et al. 2019); what is the nature and mass of BH seeds that grow to form the SMBHs of $\sim 10^8$–10^9 $M_\odot$ in the high-z Universe (Zhu et al. 2022); and what is the nature of the connection between the total mass of a host galaxy and the mass of its central SMBH (Volonteri, Habouzit & Colpi 2021).

Here, we propose a new paradigm for the nature and formation of SMBH seeds, which arise from the gravitational collapse of high-density regions of dark matter (DM) at the galaxy centres (Argüelles et al. 2021). We present calculations on the subsequent growth of such BH seeds from an accretion disc around a Kerr BH in a fully general relativistic framework. In this way, we aim here to provide answers to the above three main questions.

Among the various scenarios analysed in the literature to explain the origin of SMBHs (see Inayoshi, Visbal & Haiman 2020; Volonteri et al. 2021; Mirabel & Rodríguez 2022 for recent reviews), we can divide them into two main categories according to their formation channel: (I) channels associated with baryonic matter, i.e. gas and stars, and (II) channels associated with early Universe cosmology. In this work, we propose a novel, third possible scenario: (III) channels associated with DM. Before motivating this new framework, we highlight the pros and cons of the most studied formation channels. In the case of the baryonic channels (I), we can distinguish among (a) *Population III stars*, and (b) *direct collapse to a BH (DCBH)*. Pop. III stars are physically motivated (though yet hypothetical) stars with an average mass of $\sim 10^2\,M_\odot$ (Madau & Rees 2001; Hosokawa et al. 2016) originated in metal-free clouds hosted in small haloes of $\sim 10^6\,M_\odot$ at high z. Thus, the stellar collapse of such massive stars would lead to a BH seed of $\sim 10^2\,M_\odot$ which, under idealistic accretion conditions, would reach a $10^9\,M_\odot$ SMBH in the first billion years. However, recent state-of-the-art simulations show that BH seeds of $< 10^3\,M_\odot$ fail to grow until $10^8\,M_\odot$ at $z \sim 6$ because of strong radiative feedback (Zhu et al. 2022). In the DCBH scenario (b), dense gas clumps at the centre of massive haloes of $\sim 10^8\,M_\odot$ become globally unstable and collapse first to a supermassive star

★ E-mail: carguelles@fcaglp.unlp.edu.ar (CRA); jorge.rueda@icra.it (JAR)

of $\sim 10^4$–$10^5\,M_\odot$, which then undergoes core-collapse to a central BH. The newborn BH then grows fast by accreting surrounding material ending in a larger BH seed with masses up to $\sim$few $10^5\,M_\odot$ (Begelman, Volonteri & Rees 2006; Begelman, Rossi & Armitage 2008; Woods et al. 2017). Former simulations suggest that the conditions for the occurrence of this scenario, e.g. to reach metal-free gas able to form atomic (instead of molecular) gas, may be rare (Habouzit et al. 2016). However, recent hydrodynamic *N*-body simulations show that DCBH scenarios are among the most preferred mechanisms to explain the origin of the SMBHs (Latif et al. 2022; Zhu et al. 2022), albeit numerical resolution issues and the use of phenomenological recipes limit the generality of the results (Zhu et al. 2022).

On different physical grounds, channels of BH formation and growth associated with the early Universe (II) would take place before galaxy formation and include primordial BHs (Carr & Kühnel 2020), or even more exotic candidates such as topological defects in forms of cosmic string-loops (Bramberger et al. 2015) or domain walls (Rubin et al. 2001; Khlopov et al. 2005). However, there is no observational evidence (nor direct or indirect) of such processes since they are associated with very early cosmological epochs poorly constrained by observations.

This work proposes an SMBH formation channel in the high-z Universe conceptually different from (I) and (II) discussed above. A crucial qualitative difference with the channels mentioned above is that it does not rely either on specific pristine gas assemblies or on the very early epoch of the Universe. Instead, it depends on the gravitational collapse and subsequent growth of dense fermionic DM cores that originate at the centre of the haloes as they form. Such novel *dense core-diluted halo* DM density distributions (profiles) are natural consequences of maximum entropy production principle (MEPP) scenarios of halo formation, in which the fermionic (quantum) nature of the particles is duly accounted for Argüelles et al. (2021, 2022a). Our theory for realistic SMBH formation is original, and should not be confused with somewhat related formation scenarios via DM (of gravothermal-catastrophic nature) as porposed in (Balberg et al. 2002; Xiao H. et al. 2021) which invoke for DM self-interactions.

This paper is organized as follows. In Section 2, we discuss the underlying physics behind our new SMBH seed formation scenario and give specific examples of how such seeds may arise in the high z Universe. In Section 3, we present relativistic calculations of the time evolution of the mass and spin of the recently born BH seed with a surrounding accretion disc. We summarize and conclude in Section 4.

2 THE DARK MATTER CHANNEL OF SMBH FORMATION

The DM channel proposed for forming early BH seeds takes place within the more general and broad theory of DM halo formation as developed in Argüelles & et al. (2021) within WDM cosmologies. Unlike the (zoom-in) hydrodynamical simulation approaches applied in baryonic BH-seed formation channels (Zhu et al. 2022) (such as (Ia) and (Ib) introduced above), the problem of DM halo formation is here assessed using a thermodynamical approach for systems of self-gravitating fermions that maximize its coarse-grained entropy at the end of relaxation (Argüelles et al. 2021). This mechanism's most general density profile develops a dense and compact DM core (supported against gravity by Pauli degeneracy pressure) surrounded by a dilute halo. The first early studies of this kind of fermionic *core-halo* solutions dates back to the ′80s (Chau, Lake & Stone 1984; Ingrosso & Ruffini 1988), followed by a series of further and recent developments (Gao, Merafina & Ruffini 1990; Chavanis & Sommeria 1998; Bilic et al. 2002; Chavanis 2006; Destri, de Vega & Sanchez 2013; Argüelles & Ruffini 2014; Chavanis, Lemou & Méhats 2015; Ruffini, Argüelles & Rueda 2015; Argüelles et al. 2018, 2019; Becerra-Vergara et al. 2020, 2021; Argüelles et al. 2022b; Chavanis 2022; Krut et al. 2023). The more realistic version of this model, which includes particle evaporation and central (fermion) degeneracy, was developed in General Relativity in Argüelles et al. (2018) and is referred to as the (extended) Ruffini-Argüelles-Rueda (RAR) model.[1] The model's fermionic halo explains the galaxy rotation curves, while the degenerate fermion core has key implications for galactic centres: it can mimic a central BH or eventually collapse into one (Argüelles et al. 2018, 2019, 2021, 2022a, b; Becerra-Vergara et al. 2020, 2021). One key advantage of this semi-analytical approach is that it allows for a detailed description of the relaxed haloes from the very centre to the periphery, not possible in N-body simulations (due to limitations in resolution at inner-halo scales). Moreover, the thermodynamic approach here applied includes richer physical ingredients than those involved in traditional simulations: (i) general relativity (GR) – necessary for a proper gravitational DM core-collapse towards an SMBH seed; (ii) the quantum nature of the particles – allowing for an explicit fermion mass dependence in the profiles; (iii) the Pauli principle self-consistently included in the phase-space DF at relaxation – giving place to novel *core-halo* profiles. Interestingly, this theoretical framework allows linking the behavior and evolution of the dark matter particles from the early Universe to the late stages of non-linear structure formation at virialization. That is, the DM halo profiles are obtained by first calculating the linear matter power spectrum for $\mathcal{O}$(keV) DM fermions, to then use the corresponding extended Press–Schechter formalism to obtain the virial halo mass, $M_{\rm vir}$, with associated redshift $z_{\rm vir}$ [see the Appendix and Argüelles & et al. (2021) for a previous result]. Finally, we obtain the fermionic haloes by assuming that a MEPP takes place at the end of relaxation and agrees with the virial mass constraints. Such a MEPP, originally introduced in Chavanis (1998) generalizing Lynden-Bell results, allows obtaining a most likely coarse-grained DF of Fermi-Dirac type[2] (see equation 1 in Argüelles & et al. 2021) that depends on four free parameters, m the particle mass, β the (dimensionless) temperature, θ the degeneracy parameter, and W the cut-off particle energy. All parameters are set at the centre of the configuration (denoted with the subscript 0) to fully solve the system of equilibrium differential equations of the RAR model (see equations 8–12 in Argüelles & et al. 2021). The RAR model can be applied to form a DM halo and their central SMBH seeds.

Once having such a DF at the end of the relaxation, we calculate the full family of fermionic density profiles at equilibrium in GR, all with given total particle number N and thus with the same total (Newtonian) halo mass ($M_{\rm tot} \equiv M_{\rm vir} = mN$). For such an endeavour, we follow the thermodynamic approach applied in Argüelles et al. (2021) within the microcanonical ensemble to further calculate the important problem of (thermodynamical and dynamical) stability of such a family of equilibrium solutions. That is, not all the equilibrium

[1] It also called in the literature as the general relativistic fermionic King model (Chavanis 2022).

[2] Approaches of this kind based on statistical mechanics may present potential difficulties: the relatively short time-scale involved during violent relaxation may not be enough for the system to explore the full phase-space to reach a most likely final state (see Chavanis 2022).

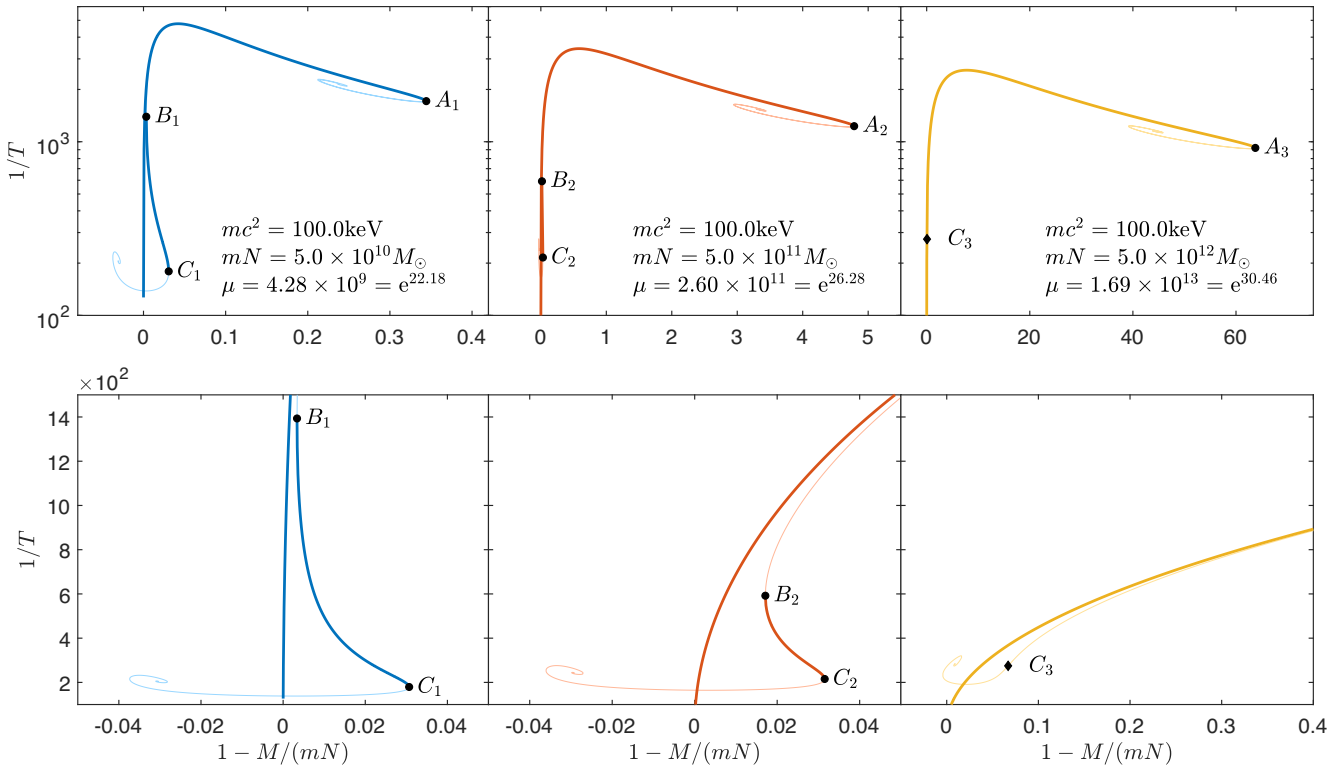

Figure 1. Caloric curves for the critical solutions of three examples with a darkino mass of $mc^2 = 100$ keV: (1) $M_{\rm vir} = 5 \times 10^{10}\,{\rm M}_\odot$ and $r_s = 30$ kpc, (2) $M_{\rm vir} = 5 \times 10^{11}\,{\rm M}_\odot$ and $r_s = 80$ kpc, (c) $M_{\rm vir} = 5 \times 10^{12}\,{\rm M}_\odot$ and $r_s = 250$ kpc. The necessary constraints ($\mu = {\rm e}^{W_0 - \theta_0}$ and N) to compute the caloric curves are extracted from the corresponding critical solutions. For the x-axis, $1 - M/(mN)$ is (minus) the binding energy normalized with mN. For the y-axis, T is the normalized temperature of the system as measured by an observer placed at infinity. Thin lines are unstable solutions, while thick lines are stable solutions. A black dot marks the change in stability. It exist a last-stable core-halo configuration located at C_1 and C_2 where the fermion core collapses towards a SMBH which is surrounded by a DM halo of astrophysical interest. The core-halo solution marked by the black diamond at C_3 has the same critical core-mass as C_1 and C_2 though is not preceded by a stable-branch .

solutions of self-gravitating fermions will be thermodynamically stable.[3] This is done following the *Katz criterium* [see Appendix A in Argüelles et al. (2021) and Appendix C in Alberti & Chavanis (2020) for updated summaries, and Katz (1978, 1979) for the original works] for which is necessary to calculate the caloric curves in GR, given as the inverse temperature of the system $1/\hat{T} \equiv \beta^{-1}$ Vs. (minus) the binding energy $-E_b = -(M - mN)c^2$ [with $\hat{T}$ the normalized temperature such that $\beta = kT/(mc^2)$ and k the Boltzmann constant]. A distinctive characteristic of such general relativistic caloric curves for fermions (at difference with the Newtonian case), is the existence of a *last stable configuration* located at the turning point (see points C_1 and C_2 in Fig. 1), followed by a second spiral feature of relativistic origin. Based on the Katz criterium, this important result was first shown in Alberti & Chavanis (2020), Chavanis (2020), Chavanis & Alberti (2020), and Chavanis (2022) for a self-gravitating system of fermions bounded in a box, together with a detailed characterization of the caloric curves and the gravitational phase transitions occurring to the Fermi gas. Remarkably, as shown as well in Argüelles et al. (2021) for the more realistic RAR (or relativistic fermionic King) model, the existence of such a *last stable configuration* located at points C_1 and C_2, implies the onset of a thermodynamical instability of the *core-halo* solutions, where the fermion-core collapses towards an SMBH.

Based on the above (relativistic) thermodynamical analysis, we demonstrate, for the first time, the existence of a critical fermion-core (located at C_i in the caloric curve) which is surrounded by a DM halo of realistic astrophysical application (see the DM density profiles in Fig. 2, concerning Fig. 1 and the fulfilment with observations in Fig. 3). We do it for a typical particle mass in the range 50–345 keV, i.e. $m = 100$ keV, to then explore (see Section 3.2) other particle masses in that range. The relevance of such a narrow window of particle masses is taken from Argüelles & et al. (2018, 2019), where it was shown it is possible to find core-halo RAR solutions where the outer halo agrees with the galaxy rotation curves while the DM core (not necessarily critical) can mimic the central BH (see also Becerra-Vergara et al. 2020, 2021; Argüelles et al. 2022b for a tailored analysis about the Milky Way and Sgr A$*$).

In Fig. 1, we give three specific examples of caloric curves for different (Newtonian) halo masses $M_{\rm vir}$ covering the relevant range between 5×10^{10}–$5 \times 10^{12}\,{\rm M}_\odot$. Among all the equilibrium *core-halo* solutions along each caloric curve, only the ones placed within the branches $B_i - C_i$ ($i = 1, 2$) are thermodynamically and dynamically stable within cosmological time-scales, as clearly explained in Argüelles et al. (2021) [see also (Alberti & Chavanis 2020; Chavanis 2020, 2022; Chavanis & Alberti 2020) for analogous results obtained for fermionic systems bounded in a box]. We recall that the *core-halo* solutions located at C_i (see Fig. 2) correspond to the last stable configuration where the DM-core achieves the

[3] While the problem of equilibrium involves the extremization of entropy $\delta S = 0$ (at fixed energy and N), the problem of stability has to do with second-order variations of entropy $\delta^2 S = 0$ Chavanis (2020).

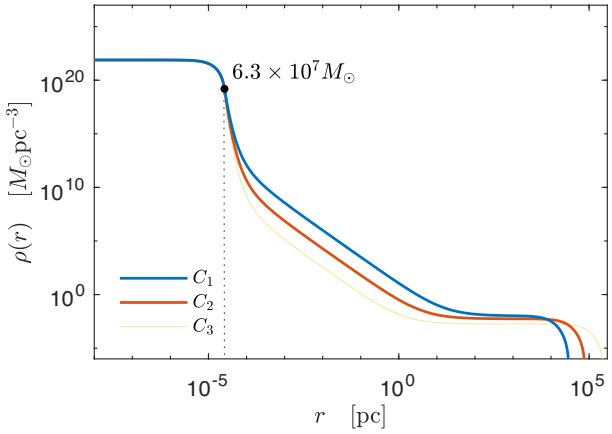

Figure 2. Core-halo density profiles corresponding to solutions C_1, C_2, and C_3 from Fig. 1, where the core has reached the critical mass for collapse into a SMBH of $M_{\rm crit} = M\,(r_c) = 6.3 \times 10^7$ M$_\odot$ (labelled with a black dot), and which are surrounded by an astrophysical halo according to Fig. 3. The dotted line shows the corresponding fully degenerate core solution, from which we define the core radius $r_{\rm c}$ of the more general semi-degenerate core-halo profiles here analyzed.

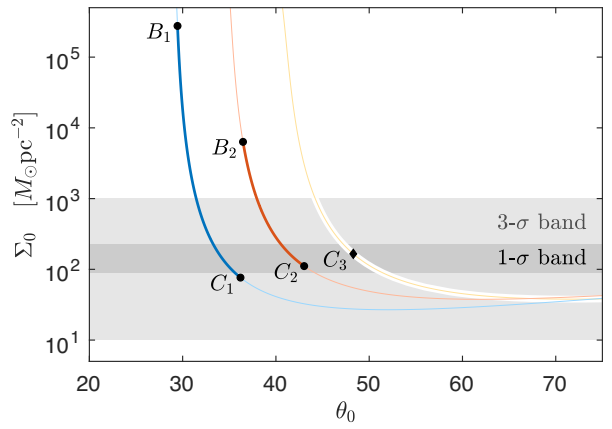

Figure 3. Surface DM density curves as a function of central fermion degeneracy (θ_0), for three examples as described Fig. 1. Thin lines are unstable solutions, while thick lines between $B_i - C_i$ are meta-stable. The shaded regions mark the maximal extent of 1σ and 3σ errors as obtained in Donato et al. (2009), evidencing the astrophysical validity of the fermionic haloes which surround the critical cores associated to each $C_{\rm i}$ solution.

onset of gravitational collapse (of relativistic origin) towards a BH. Interestingly, at the fixed mass of $m = 100$ keV, the theory predicts a threshold total halo mass $M_{\rm vir} \sim 5 \times 10^{12}$ M$_\odot$ above which the stable branch $B_3 - C_3$ disappeared (see the right-hand panels of Fig. 1). The shrinking of the metastable branch ($B - C$) as the total mass $M_{\rm tot}$ (or N) increases; together with the existence of a threshold particle number N^* above which the meta-stable branch disappear, was first shown in Alberti & Chavanis (2020) and Chavanis & Alberti (2020) for box confined systems. This remarkable result, when applied to realistic haloes as in this work, may explain why we do not observe single virialized galaxies above such an order of magnitude (i.e. above $\mathcal{O}(10^{12})$ M$_\odot$), indicating how powerful the thermodynamics of self-gravitating systems can be.

Moreover, in such a halo-mass window, we further show in Fig. 3 that the halo regime of the RAR solutions has the required morphology in the sense of being able to fulfil the DM surface density relation. We also show in Fig. 2 the density profiles of such core-halo astrophysical solutions at the onset of DM core-instability, all having a typical SMBH seed of $M_{\rm crit} \approx 6.3 \times 10^7$ M$_\odot$. We have defined the SMBH seed mass at the core radius r_c of the core-halo solution, i.e. $M_{\rm crit} = M(r_c)$, with r_c coinciding with the surface radius of the corresponding fully degenerate solution (e.g. where the density falls to zero, see dotted line in Fig. 2). Such a numerical value of the critical mass can be well approximated with the semi-analytic equation (1) (only valid within the fully degenerate regime), which is no other than the Oppenheimer-Volkoff (OV) mass limit Oppenheimer & Volkoff (1939)

$$M_{\rm crit} \approx 0.384 \frac{m_{\rm Pl}^3}{m^2} \approx 6.274 \times 10^9 \left(\frac{10\,\mathrm{keV}}{mc^2}\right)^2 \mathrm{M}_\odot, \tag{1}$$

where $m_{\rm Pl} = \sqrt{\hbar c/G} \approx 2.176 \times 10^{-5}$ g is the Planck's mass and m is the darkino mass.

The reason for the validity of this critical mass approximation of our DM cores can be easily understood when realizing that the core-halo fermionic solutions under consideration here (see Fig. 2) encompass two different regimes: a highly degenerate (quantum) regime of the fermionic-core (i.e. $\theta_0 > 10$) close to the fully degenerate case, which monotonically transitions to the classical regime at larger distances from the centre, leading to the (Boltzmannian) halo region [where $\theta(r) \ll -1$]. Further detailed explanations about the equivalence between the traditional turning-point instability criterium of core-collapse Schiffrin & Wald (2014), to that of the last (dynamical and thermodynamical) stable solution at point C_i in the caloric curves are given in section 4 of Argüelles et al. (2021) and references therein.

3 BH MASS AND SPIN EVOLUTION

We follow the treatment of a nearly geodesic thin accretion disc around a Kerr BH in Novikov & Thorne (1973), Page & Thorne (1974), and Thorne (1974). Matter and radiation transfer energy and angular momentum to the BH during the accretion. In particular, it is essential to account for the feedback of radiation/photons on to the BH since they exert a counter-torque Godfrey (1970) that avoids the BH from reaching the extreme regime $a = M$. This implies that the accretion of massive particles and radiation does not lead the BH to become a naked singularity (Thorne 1974). We denote by dm the rest-mass accreted by the BH in a coordinate time interval dt, so $\dot{m} = \mathrm{d}m/\mathrm{d}t$ is the rest-mass accretion rate, and $\dot{M}_{\rm rad}$ and $\dot{J}_{\rm rad}$ are the rate of energy and angular momentum transfer by radiation to the BH. We refer the reader to the Appendix B for details of the equations governing the evolution of the mass and angular momentum of the BH. We use geometric units $c = G = 1$ unless otherwise specified.

3.1 Accretion rate and luminosity

We calculate the rate at which rest-mass flows inwards through the local balance between the tidal gravitational acceleration and the radiation pressure along the z coordinate. This condition is

$$z R^{\bar{z}}_{\bar{0}\bar{z}\bar{0}} = \kappa F(r), \tag{2}$$

where $\kappa = 0.34$ cm^2 g^{-1} is the Thomson electron scattering opacity, $\boldsymbol{R}$ is the Riemann tensor. Using the change of variable $x = \sqrt{r/M}$, equation (2) becomes

$$\frac{3\kappa\,\dot{m}}{8\pi z} f(x, \alpha) = 1, \tag{3}$$

where

$$f(x,\alpha) = \frac{x^3\, g(x,\alpha)}{x^4 - 4\alpha x + 3\alpha^2}, \tag{4}$$

and

$$g(x,\alpha) = x - x_0 - \frac{3}{2}\alpha \ln\left(\frac{x}{x_0}\right) - 3(A_1 + A_2 + A_3), \tag{5}$$

with

$$A_1 = \frac{(x_1-\alpha)^2}{x_1(x_1-x_2)(x_1-x_3)} \ln\left(\frac{x-x_1}{x_0-x_1}\right). \tag{6}$$

Here, x_1, x_2, x_3 are the roots of the polynomial $x^3 - 3x + 2a$. The terms A_2 and A_3 can be obtained from A_1 through a cyclic order of the set $\{1, 2, 3\}$. For a given value of α and an appropriate expression $z = z(r)$, the value of $\dot{m}$ such that equation (3) has exactly one solution defines a critical accretion rate $\dot{m}_{\rm crit}$. Above this rate, the disc enters the super-Eddington regime, and the thin disc approximation breaks down. The tidal gravitational pull reaches a maximum value at $z = H$. Additionally, the thin disc approximation is reasonably accurate insofar as the half thickness of the disc obeys $H < r$ (Chen & Beloborodov 2007; Liu, Gu & Zhang 2017). Consequently, by introducing a parameter $0 < \beta \leq 1$ (not to be confused with the dimensionless temperature parameter introduced in Section 2) and setting $z = r$ (see Abolmasov & Chashkina 2015 for details), we calculate the accretion rate by

$$\dot{m} \equiv \beta\, \dot{m}_{\rm crit} = \frac{8\pi\beta M}{3\kappa \max\left\{\frac{f(x,\alpha)}{x^2}\right\}}, \tag{7}$$

with $\max\left\{\frac{f(x,\alpha)}{x^2}\right\}$, the maximum value can take the given function at each radius for given α. To calculate the power emitted by the system, we only consider the photons that leave the disc and do not fall into the BH. The procedure is equivalent to calculating the rate of energy transfer to the BH, i.e. equation (B5), but using the factor $1 - C$ instead of C

$$L_{\rm source} = -\frac{2}{\pi}\int_{r_0}^{\infty}\int_0^{\pi/2}\int_0^{2\pi}(1-C)\, k_t F(r) {\rm d}S. \tag{8}$$

We do not consider the possible photon recapture by the disc.

3.2 Growth of Kerr BH seeds

The equations of evolution are

$$\dot{M} = \dot{m}\epsilon_0 + \dot{M}_{\rm rad}, \tag{9}$$

$$\dot{\alpha} = \tfrac{1}{M^2}\left(l_0\dot{m} + \dot{J}_{\rm rad} - 2M\dot{M}\alpha\right). \tag{10}$$

It is helpful to make the M dependence explicit and express the equations in terms of the system's parameters and dimensionless variables. To that end, let us write

$$M = M_i \tilde{M}, \tag{11}$$

$$\dot{m} = M_i \tilde{M}\beta\dot{\tilde{m}}, \tag{12}$$

$$\dot{M}_{\rm rad} = M_i \tilde{M}\beta\dot{\tilde{m}}\tilde{M}_{\rm rad}, \tag{13}$$

$$\dot{J}_{\rm rad} = M_i^2 \tilde{M}^2\beta\dot{\tilde{m}}\tilde{J}_{\rm rad}, \tag{14}$$

$$l_0 = M_i \tilde{M}\tilde{l}_0, \tag{15}$$

where $\dot{\tilde{m}}$, $\tilde{M}_{\rm rad}$, $\tilde{J}_{\rm rad}$ and $\tilde{l}_0$ are functions of α only. With these definitions, the ratio between equations (9) and (10) leads to the solution

$$\tilde{M} = \exp\left\{\int_{\alpha_i}^{\alpha} \frac{\epsilon_0 + \tilde{M}_{\rm rad}}{\tilde{l}_0 + \tilde{J}_{\rm rad} - 2\alpha_*\left(\epsilon_0 + \tilde{M}_{\rm rad}\right)} {\rm d}\alpha_*\right\}, \tag{16}$$

for the BH mass as a function of the dimensionless spin parameter. From equation (10), we obtain

$$\Delta t = \frac{1}{\beta}\int_{\alpha_i}^{\alpha} \frac{1}{\dot{\tilde{m}}\left[\tilde{l}_0 + \tilde{J}_{\rm rad} - 2\alpha_*\left(\epsilon_0 + \tilde{M}_{\rm rad}\right)\right]} {\rm d}\alpha_*. \tag{17}$$

From equations (16) and (17), we can deduce some properties of the BH's temporal evolution: The solution $\alpha(t)$ is independent of M, but it does depend on the parameter β. Moreover, the general solution $\alpha(t, \beta)$ obeys the relation $\alpha(t, \beta) = \alpha(\beta t, 1)$. The BH mass inherits this property through equation (16), and we get $M(t, \beta) = M(\beta t, 1)$. The same will happen with any α and M function. This behaviour suggests that knowing the solution for $\beta = 1$ is enough to produce other solutions by properly scaling the variable t and multiplying it by an adequate power of β. For example, the accretion rate and the power emitted obey the relations $\dot{m}(t, \beta) = \beta\dot{m}(\beta t, 1)$ and $L_{\rm source}(t, \beta) = \beta L_{\rm source}(\beta t, 1)$.

The properties of $M(t, \beta)$ and $\alpha(t, \beta)$ become evident when inspecting the panels in Fig. 4, where we show the evolution of several BH seeds for values $\beta = 1$, $\beta = 0.1$, and $\beta = 0.01$ as a function of time and the cosmological redshift. The initial redshift z_0 corresponds to the typical collapse z^* of a gravitationally bound object with mass $M_{\rm vir}$ in the extended Press–Schechter formalism (see Appendix A). The standard Lambda cold dark matter (ΛCDM) cosmology sets the relation between t and z. Note that $\alpha(t, \beta)$ does not depend on the BH mass, so the top left-hand panel contains only three curves, one for each value of β.

In Fig. 5, we show the evolution of the accretion rate and the power emitted by the BH. The slight reduction in the accretion rate for small values of t occurs because the factor $\max\{f(x, \alpha)/x^2\}$ in equation (7) increases by a factor of $\sim$5 as α grows. The spin-up of a BH from $\alpha_i = 0$ to $\alpha = 0.99775$ takes $\sim 37/\beta$ Myr. The BH mass grows from M_i to $\sim 3M_i$. Once α reaches the state $\dot{\alpha} \approx 0$, the BH mass grows exponentially. By solving equation (9), we find a relation that allows us to estimate the time Δt needed for any BH seed to grow up to a final mass $M_f > 3M_i$, starting from $\alpha_i = 0$:

$$\Delta t = 6.2 \times 10^7 \ln\left\{\frac{3M_f}{5M_i}\right\}\beta^{-1}\ {\rm yr}. \tag{18}$$

Our result differs from equation 1 in Haiman & Loeb (2001), namely,

$$\Delta t_{\rm HL} = 4 \times 10^8 \varepsilon \ln\left\{\frac{M_f}{M_i}\right\}\beta^{-1}\ {\rm yr}, \tag{19}$$

where $\varepsilon = L_{\rm source}/\dot{m}c^2$ is the radiative efficiency of the accretion process. The differences arise for two reasons: first, Haiman & Loeb (2001) did not consider the BH spin, while our treatment accounts for it in a self-consistent manner: Fig. 4 shows that during the transition to a saturated spin, the BH growth is faster than exponential. Secondly, their definition of the accretion rate rests upon a *global* balance between Newtonian gravity and spherically symmetric radiation pressure. Consequently, the radiative efficiency appears as a constant factor in equation (19). Our definition adopts a relativistic *local* balance between radiation pressure and vertical gravity, which increases the accretion rate (Abolmasov & Chashkina 2015) and allows the evolution of the efficiency with the BH parameters M and α.

Using the limiting efficiency for a Kerr BH, $\varepsilon = 0.3$, we obtain $\Delta t < 0.52\Delta t_{\rm HL}$. Thus, the growth from a possible BH seed within

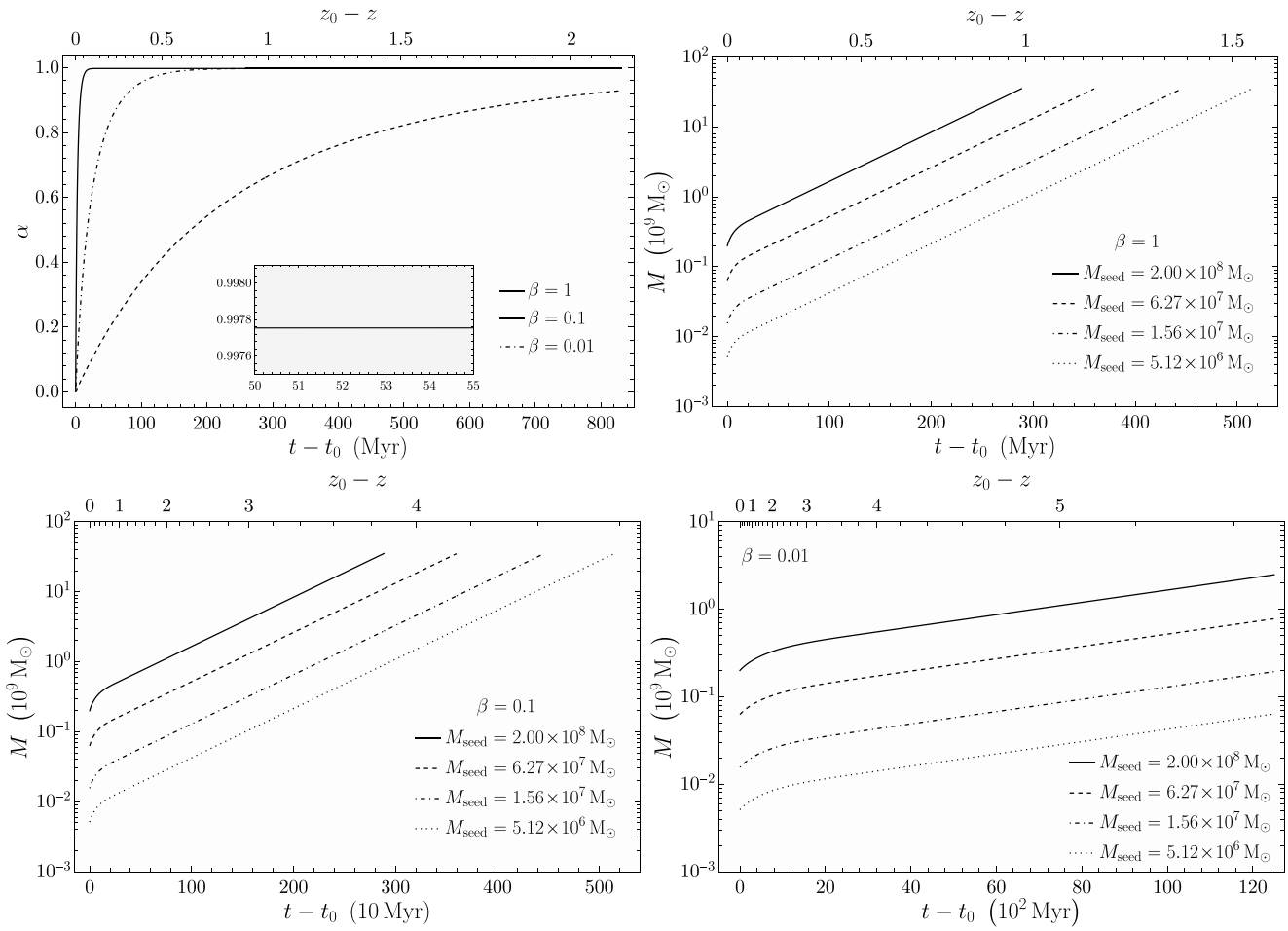

Figure 4. BH evolution in time for different BH seeds and values of β. Initial conditions are $\alpha_i = 0$ and darkino masses 56, 100, 200, and 350 keV. The spin parameter does not depend on the BH mass. The initial redshift is $z_0 = 5.5$ with $t_0 = 1022$ Myr for a halo mass $M_{\rm vir} = 5 \times 10^{11}M_\odot$.

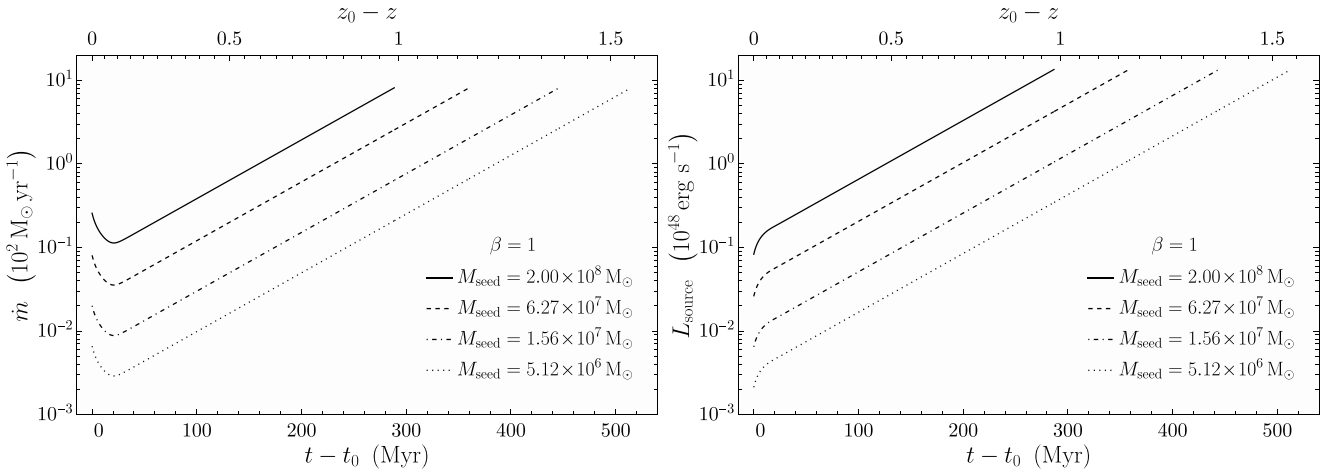

Figure 5. Accretion rate and luminosity at source as functions of t for different BH seeds with $\beta = 1$. Initial conditions are $\alpha_i = 0$ and darkino masses 56, 100, 200, and 350 keV. The initial redshift is $z_0 = 5.5$ with $t_0 = 1022$ Myr for a halo mass $M_{\rm vir} = 5 \times 10^{11}M_\odot$.

our framework of $M_i = 5 \times 10^6$M$_\odot$ to $M_f = 5 \times 10^9$M$_\odot$ takes only $\Delta t \approx 0.4$ Gyr. In particular, our DM channel for SMBH formation predicts that typical DM haloes of $M_{\rm vir} \sim 10^{11}$ M$_\odot$ formed at $z_0 \sim 7.5$ (see Appendix A) can harbour SMBH seeds of $M_i = 6.3 \times 10^7$ M$_\odot$ (i.e. for $m = 100$ keV), which can grow (within standard accretion rates) up to $M_f \equiv M = 3 \times 10^9$ M$_\odot$ in $\Delta t \approx 0.2$ Gyr, thus in agreement with most distant (i.e. $z \sim 6$) and most massive quasars observed (see e.g. Mirabel & Rodríguez 2022). This result provides

a new channel for SMBH formation from DM which can overcome traditional baryonic scenarios such as Pop. III stars, whose light BH seeds of $< 10^3\,M_\odot$ fail to grow even to $\sim 10^8\,M_\odot$ by $z \sim 6$ (Zhu et al. 2022).

4 CONCLUSIONS

We have proposed a novel channel for SMBH formation in the high redshift Universe, which is not associated with baryonic matter (massive stars) or primordial cosmology. Instead, it relies on the gravitational collapse into a BH of fermionic dense DM cores that arise at the centre of DM haloes as they form and on the subsequent growth of the newborn BH by accretion. The formation of dense core-dilute halo density distributions of DM form when accounting for a fermionic (quantum) nature of the DM particles in the structure of the DM haloes, which is not feasible in traditional N-body simulations Argüelles & et al. (2021); Argüelles et al. (2022a). For fermion masses in the range of 50–345 keV, this alternative non-linear structure formation approach predicts stable DM haloes that agree with observations and harbor dense DM cores at the brink of gravitational collapse, with masses on the range of 10^6–$10^8\,M_\odot$ (see Section 2 for a WDM cosmology with $m = 100$ keV). Thus, it offers a whole new range of SMBH seeds that are considerably larger than the ones predicted by baryonic formation channels, including the DCBH scenario (see Section 1).

In this article, we assessed the mass and angular momentum evolution of such massive BH seeds using a standard, geodesic general relativistic disc accretion model. We self-consistently account for the feedback of radiation/photons onto the BH (see Section 3). We have explicitly shown in Section 4 that these SMBH can grow to masses in the range $\sim 10^9$–$10^{10}\,M_\odot$ within the first Gyr of the life of the Universe, in good agreement with the farthest quasars observed, without invoking unrealistic (or fine-tuned) accretion rates. A relevant advantage of the present framework is that it does not require star formation within such a short cosmological time scale as in traditional baryonic channels. At the same time, it naturally connects the total mass of a host galaxy and the mass of its central SMBH observed today, all in terms of DM and its cosmological evolution.

ACKNOWLEDGEMENTS

CRA was supported by CONICET of Argentina, the ANPCyT (grant PICT-2018-03743), and ICRANet. KB acknowledges partial support from the Science Committee of the Ministry of Science and Higher Education of the Republic of Kazakhstan (grant no. AP19680128).

DATA AVAILABILITY

The article's data will be shared with the corresponding author upon reasonable request.

REFERENCES

Abolmasov P., Chashkina A., 2015, MNRAS, 454, 3432
Adhikari R. et al., 2017, JCAP, 2017, 25
Alberti G., Chavanis P.-H., 2020, Eur. Phys. J. B, 93, 208
Argüelles C. R. et al., 2018, Phys. Dark Universe, 21, 82
Argüelles C. R. et al., 2019, Phys. Dark Universe, 24, 100278
Argüelles C. R. et al., 2021, MNRAS, 502, 4227
Argüelles C. R., Becerra-Vergara E. A., Krut A., Yunis R., Rueda J. A., Ruffini R., 2022a, Int. J. Mod. Phys. D, 31, 2230002
Argüelles C. R., Mestre M. F., Becerra-Vergara E. A., Crespi V., Krut A., Rueda J. A., Ruffini R., 2022b, MNRAS, 511, L35
Argüelles C. R., Ruffini R., 2014, Int. J. Mod. Phys. D, 23, 1442020
Balberg S. et al., 2002, ApJ, 568, 475
Bardeen J. M., 1973, Timelike and null geodesics in the Kerr metric, in Black Holes. Les Astres Occlus, Les Houches, France, pp. 215–239
Becerra-Vergara E. A. et al., 2020, A&A, 641, A34
Becerra-Vergara E. A. et al., 2021, MNRAS, 505, L64
Begelman M. C., Rossi E. M., Armitage P. J., 2008, MNRAS, 387, 1649
Begelman M. C., Volonteri M., Rees M. J., 2006, MNRAS, 370, 289
Bilic N., Munyaneza F., Tupper G. B., Viollier R. D., 2002, Prog. Part. Nucl. Phys., 48, 291
Binney J., Tremaine S., 2008, Galactic Dynamics, 2nd edn. Princeton Univ. Press, Princeton
Bode P., Ostriker J. P., Turok N., 2001, ApJ, 556, 93
Boshkayev K., Idrissov A., Luongo O., Malafarina D., 2020, MNRAS, 496, 1115
Boshkayev K., Konysbayev T., Kurmanov E., Luongo O., Malafarina D., Quevedo H., 2021, Phys. Rev. D, 104, 084009
Boyarsky A., Drewes M., Lasserre T., Mertens S., Ruchayskiy O., 2019, Prog. Part. Nucl. Phys., 104, 1
Bramberger S. F., Brandenberger R. H., Jreidini P., Quintin J., 2015, J. Cosm. Astropart. Phys., 2015, 007
Bryan G. L., Norman M. L., 1997, ApJ, 495, 80
Bullock J. S., Boylan-Kolchin M., 2017, Ann. Rev. Astron. Astrophys., 55, 343
Carr B., Kühnel F., 2020, Ann. Rev. Nucl. Part. Sci., 70, 355
Chau W. Y., Lake K., Stone J., 1984, ApJ, 281, 560
Chavanis P. H., 2006, Int. J. Mod. Phys. B, 20, 3113
Chavanis P. H., Sommeria J., 1998, MNRAS, 296, 569
Chavanis P.-H., 1998, MNRAS, 300, 981
Chavanis P.-H., 2020, Eur. Phys. J. Plus, 135, 290
Chavanis P.-H., 2022, Phys. Rev. D, 106, 043538
Chavanis P.-H., Alberti G., 2020, Phys. Lett. B, 801, 135155
Chavanis P.-H., Lemou M., Méhats F., 2015, Phys. Rev. D, 92, 123527
Chen W.-X., Beloborodov A. M., 2007, ApJ, 657, 383
Destri C., de Vega H. J., Sanchez N. G., 2013, New A, 22, 39
Donato F. et al., 2009, MNRAS, 397, 1169
Fitts A. et al., 2019, MNRAS, 490, 962
Gao J. G., Merafina M., Ruffini R., 1990, A&A, 235, 1
Godfrey B. B., 1970, Phys. Rev. D, 1, 2721
Habouzit M., Volonteri M., Latif M., Dubois Y., Peirani S., 2016, MNRAS, 463, 529
Haiman Z., Loeb A., 2001, ApJ, 552, 459
Hosokawa T., Hirano S., Kuiper R., Yorke H. W., Omukai K., Yoshida N., 2016, ApJ, 824, 119
Inayoshi K., Visbal E., Haiman Z., 2020, ARA&A, 58, 27
Ingrosso G., Ruffini R., 1988, Nuovo Cimento B Serie, 101, 369
Karukes E. V., Benito M., Iocco F., Trotta R., Geringer-Sameth A., 2019, J. Cosm. Astropart. Phys., 2020, 033
Katz J., 1978, MNRAS, 183, 765
Katz J., 1979, MNRAS, 189, 817
Khlopov M. Y. et al., 2005, Astroparticle Physics, 23, 265
Kolb E. W., Turner M. S., 1990, The Early Universe. Frontiers in Physics, Westview Press, Boulder, CO, https://cds.cern.ch/record/206230
Krut A., Argüelles C. R., Chavanis P. H., Rueda J. A., Ruffini R., 2023, ApJ, 945, 1
Latif M. A., Whalen D. J., Khochfar S., Herrington N. P., Woods T. E., 2022, Nature, 607, 48
Liu T., Gu W.-M., Zhang B., 2017, New Astron. Rev., 79, 1
Lovell M. R. et al., 2012, MNRAS, 420, 2318
Macciò A. V., Paduroiu S., Anderhalden D., Schneider A., Moore B., 2012, MNRAS, 424, 1105
Madau P., Rees M. J., 2001, ApJ, 551, L27
Mirabel I. F., Rodríguez L. F., 2022, New A Rev., 94, 101642
Mo H., van den Bosch F., White S., 2010, Galaxy Formation and Evolution. Cambridge Univ. Press, Cambridge
Navarro J. F., Frenk C. S., White S. D. M., 1997, Astrophys.J., 490, 493

Novikov I. D., Thorne K. S., 1973, in DeWitt C., DeWitt B., eds, Black Holes (Les Astres Occlus), p. 343, Gordon and Breach, N.Y.
Oppenheimer J. R., Volkoff G. M., 1939, Phys. Rev., 55, 374
Page D. N., Thorne K. S., 1974, ApJ, 191, 499
Press W., Schechter P., 1974, ApJ, 187, 425
Rubin S. G. et al., 2001, J. Exp. Theor. Phys., 92, 921
Rueda J. A., Ruffini R., Kerr R. P., 2022, ApJ, 929, 56
Ruffini R., Argüelles C. R., Rueda J. A., 2015, MNRAS, 451, 622
Schiffrin J. S., Wald R. M., 2014, Class. Quantum Grav., 31, 035024
Thorne K. S., 1974, ApJ, 191, 507
Viel M., Becker G., Bolton J., Haehnelt M., 2013, Phys. Rev. D, 88, 43502
Volonteri M., 2012, Science, 337, 544
Volonteri M., Habouzit M., Colpi M., 2021, Nature Rev. Phys., 3, 732
Woods T. E. et al., 2019, PASA, 36, e027
Woods T. E., Heger A., Whalen D. J., Haemmerlé L., Klessen R. S., 2017, ApJ, 842, L6
Xiao H. et al., 2021, J. Cosm. Astropart. Phys., 2021, 039
Yunis R., Argüelles C. R., Scóccola C. G., Nacir D. L., Giordano G., 2021, J. Cosm. Astropart. Phys.
Zhu Q., Li Y., Li Y., Maji M., Yajima H., Schneider R., Hernquist L., 2022, MNRAS, 514, 5583

APPENDIX A: DM HALO FORMATION SCALES WITHIN THE PRESS–SCHECHTER PARADIGM

In the context of the calculation of solutions that represent fermionic DM haloes via the MEPP, as shown in Section 2 and initially developed in Argüelles et al. (2021), a key parameter comes from the boundary conditions for the solutions, for these general quasi-equilibrium solutions can only describe DM haloes if their masses and radii correspond to the ones characteristic of such structures (Argüelles et al. 2018, 2019). Indeed, the conclusions of such analysis regarding the thermodynamic stability of this system are susceptible to such contour conditions, with other authors reaching different conclusions by using the same analysis when considering systems smaller than galactic haloes (Chavanis et al. 2015; Alberti & Chavanis 2020). Thus, appropriately choosing the mass and radius corresponding to a galactic halo becomes important. While DM halo masses are usually a well-estimated observable for most observed structures Karukes et al. (2019), defining the radius of such structures can depend on the particular cosmological model considered [see e.g. Mo, van den Bosch & White (2010) for a thorough explanation]. A common measure for such radii is the virial radius, obtained from applying the virial theorem to the gravitationally bound structure. However, due to differences arising from the particular collapse models used, it is common to use instead the r_{200} radius, defined as the radius where the density of the system is 200 times the background DM density (Binney & Tremaine 2008), which is close to the value of the virial radius $r_{\rm vir}$ for most models (Bryan & Norman 1997). Thus, the relation between mass and r_{200} radius for these structures is relatively straightforward:

$$M_{\rm vir} = 200\frac{4}{3}\pi r_{200}^3\rho_c(t) = 100\frac{H_0^2 r_{200}^3[1+z(t)]^3}{G}\,, \tag{A1}$$

where $M_{\rm vir}$ stands for the (virial) mass of the object. We see, however, that this definition is now time-dependent, as the background density of the Universe evolves with time. In a cosmological context, we can also reinterpret this time dependence as the expansion of the spatial scales involved in the problem with time.

To marginalize this time dependence, a first approach can be to estimate the most likely collapse time of a structure of size $M_{\rm vir}$ and obtain the physical radius corresponding to such scale. While a deep study of this collapse time would typically involve a full study on nonlinear cosmology and structure formation (such as e.g. Navarro, Frenk & White 1997; Macciò et al. 2012; Fitts et al. 2019), it is sufficient for this study to use the Press–Schecter formalism (Press & Schechter 1974), based on the results from linear cosmology for a given model. This is a well-studied theory, and a full description can be found, for example, in Binney & Tremaine (2008); Mo et al. (2010) among many other works. Here, we will limit ourselves to a summary of the assumptions and results. To study this formalism, it is necessary first to study how the overdensities collapse in the late, matter-dominated Universe. For this, we can use one of the simpler nonlinear collapse models, the spherical collapse (see e.g. Mo et al. 2010). Under the assumptions of this model, any given overdensity collapses to form a virialized structure, and at that point, the linear theory of perturbation evolution will predict an overdensity of $\delta_c \sim 1.69$. So, according to this theory, we can assume that given an overdensity field evolving according to linear dynamics, a peak of density $>\delta_c$ would instead correspond to a collapsed halo. The core assumption of Press–Schechter's formalism regards how to relate this observation to the halo mass function. The formalism proposes that the fraction of the Universe's total mass that is in haloes of masses greater than M is equal to the probability of a given overdensity is greater than the critical δ_c, where the overdensity field δ_M(t) is averaged with a filter of characteristic mass M. For this study, knowing the exact mass fraction of a given mass M is not important. Instead, we are interested in the characteristic timescale at which overdensities of mass M are most likely to collapse. In this case, we can assume most overdensities will start to collapse when the standard deviation σ_M of the Gaussian field δ_M (known as the *mass variance*) crosses the threshold of δ_c. Thus, for an overdensity of mass M, we define a characteristic collapse time as

$$\sigma_M(z^*) = \delta_c, \tag{A2}$$

where

$$\sigma_M^2(t) = \frac{1}{2\pi^2}\int_0^\infty P(k)D^2(t)W^2(k,R)k^2{\rm d}k, \tag{A3}$$

being $D(t)$ the linear growth rate of perturbations, $P(k)$ the linear matter power spectrum, $W(k, R)$ a window function of characteristic radius $R(M)$ (taken as a *top hat function* here, see e.g. Mo et al. 2010), and $\delta_c \simeq 1.69$ according to spherical collapse (Mo et al. 2010).

We note that to obtain this characteristic collapse mass, it is necessary to know the linear matter power spectrum, typically obtained through a study on a particular cosmological model. In the preceding sections, we have seen a particle mass-dependent description of DM halo formation, where these masses are of order $\mathcal{O}$ 100 keV. This particle mass is significantly lighter than most CDM models suggest (Kolb & Turner 1990); and instead points to an extension of the standard ΛCDM theory known as warm dark matter (WDM) Bode, Ostriker & Turok (2001); Lovell et al. (2012); Boyarsky et al. (2019). These types of extensions, typically characterized by DM particle masses in the keV ranges, show a considerably higher initial velocity dispersion when compared to their standard CDM counterparts, which in turn predicts a smaller number of small-scale structures in the Universe and may alleviate some existing tensions with CDM (Bullock & Boylan-Kolchin 2017). The simplest production scenario for WDM is that these particles are created via thermal processes very early in the Universe's history, and indeed this production scenario requires some degrees of freedom in the initial plasma well above 10^3 Mo et al. (2010). In any case, this scenario is an interesting benchmark for other production scenarios, as most result in a similar suppression feature in the matter power spectrum. An interesting class of models that can realize this WDM scenario can be found in sterile neutrino WDM, where non-equilibrium production of these particles

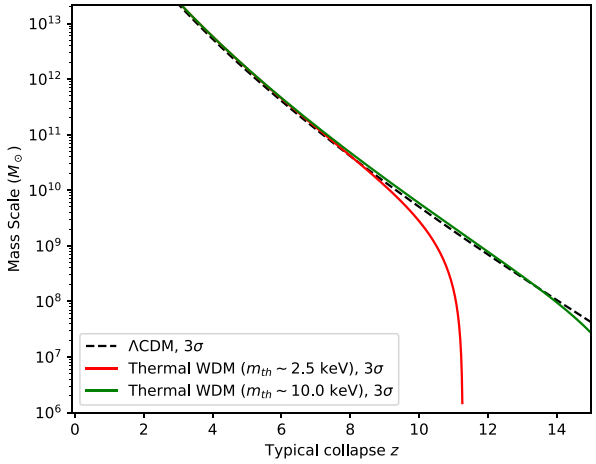

Figure A1. Characteristic collapse redshift z^* as a function of substructure mass M. CDM models are represented in black lines, and WDM thermally produced relic models with $mc^2 = 2.5$ keV and $mc^2 = 10.0$ keV in red, blue, and green, respectively. The models considered here are taken at the 3σ threshold in the sense of equation (A3), as an estimation of the earliest possible haloes.

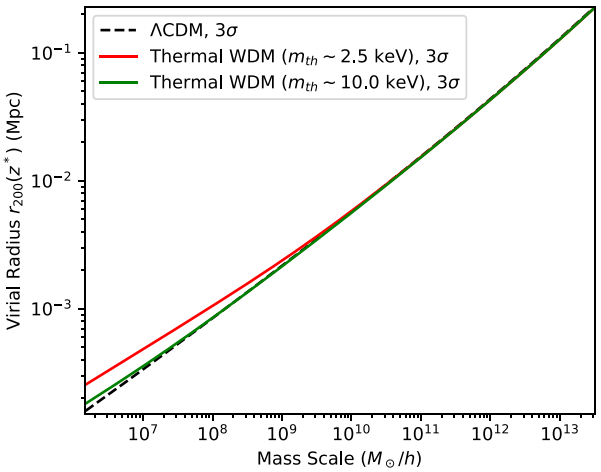

Figure A2. Virial radius r_{200} at virialization time as a function of substructure mass M. CDM models are represented in black lines and WDM thermally produced relic models with $mc^2 = 2.5$ keV, $mc^2 = 5.0$ keV, and $mc^2 = 10.0$ keV in red, blue, and green, respectively. The models considered here are taken at the 3σ threshold in the sense of equation (A3), as an estimation of the earliest possible haloes.

can account for the observed DM fraction (Adhikari et al. 2017; Boyarsky et al. 2019), and particle self-interaction can reconcile the parameter space of these models with observation Yunis et al. (2021).

We can see the results for the r_{200} as a function of the halo mass scale M in figure Fig. A2 according to the Press–Schechter formalism, while the typical collapse redshift z∗ as a functiof M is given in Fig. A1, calculated for three thermally produced WDM models as well as a standard ΛCDM model. For reference, these 2.5 and 10 keV thermal models have similar suppression features as ∼15 and 100 keV non-resonantly produced sterile neutrinos, according to the criteria of Viel et al. (2013). We also include a line representing a CDM model, but where equation (A3) has been refactored with 3σ instead to represent the time when earliest collapsed structures in the formalism are formed. There are thought to be produced roughly when rare 3σ overdensities cross the δ_c barrier and enter nonlinear collapse. However, in the mass scales relevant to these studies, the differences in r_{200} between WDM and CDM models are minimal, and these cosmologies can be used interchangeably to calculate DM halo solutions.

APPENDIX B: GEODESIC DISC ACCRETION

We here present the equations of the evolution of a Kerr BH during the accretion of matter from a geodesic thin disc. The treatment closely follows the formulation in Novikov & Thorne (1973), Page & Thorne (1974), and Thorne (1974).

In the equatorial plane ($\theta = \pi/2$) and close above it, the Kerr spacetime metric can be written as

$$ds^2 = -e^{2\nu}dt^2 + e^{2\psi}(d\phi - \omega dt)^2 + e^{2\mu}dr^2 + dz^2, \tag{B1}$$

where z is the height above the equatorial plane, and ν, ψ, μ, ω are functions of the radial coordinate r:

$$e^{2\nu} = \frac{r^2\Delta}{A}, \quad e^{2\psi} = \frac{A}{r^2}, \quad e^{2\mu} = \frac{r^2}{\Delta}, \quad \omega = \frac{2Mar}{A}, \tag{B2}$$

being $\Delta = r^2 - 2Mr + a^2$, and $A = (r^2 + a^2)^2 - \Delta a^2$, with M and $a = J/M$, respectively, the BH mass and angular momentum per unit mass.

Matter and radiation transfer energy and angular momentum to the BH during the accretion. In particular, it is essential to account for the feedback of radiation/photons onto the BH since they exert a counter-torque Godfrey (1970) that avoids the BH from reaching the extreme regime $a = M$. This implies that the accretion of massive particles and radiation does not lead the BH to become a naked singularity Thorne (1974). We denote by dm the rest-mass accreted by the BH in a coordinate time interval dt, so $\dot{m} = dm/dt$ is the rest-mass accretion rate, and $\dot{M}_{\rm rad}$ and $\dot{J}_{\rm rad}$ are the rate of energy and angular momentum transfer by radiation to the BH. Therefore, we can write the BH energy and angular momentum conservation equations as Thorne (1974)

$$\dot{M} = \dot{M}_{\rm matter} + \dot{M}_{\rm rad}, \tag{B3}$$

$$\dot{J} = \dot{J}_{\rm matter} + \dot{J}_{\rm rad}, \tag{B4}$$

where

$$\dot{M}_{\rm matter} = \epsilon_0 \dot{m}, \tag{B5}$$

$$\dot{J}_{\rm matter} = l_0 \dot{m}, \tag{B6}$$

$$\dot{M}_{\rm rad} = -\frac{2}{\pi}\int_{r_0}^{\infty}\int_0^{\pi/2}\int_0^{2\pi} C k_t F(r) dS, \tag{B7}$$

$$\dot{J}_{\rm rad} = \frac{2}{\pi}\int_{r_0}^{\infty}\int_0^{\pi/2}\int_0^{2\pi} C k_\phi F(r) dS, \tag{B8}$$

being ϵ_0 and l_0 the specific (i.e. per unit mass) energy and angular momentum of the matter accreted, i.e. at the radius r_0 of the innermost stable circular orbit (ISCO). Assuming that radiation emitted from the disc's surface is isotropic, the normalized photon four-momentum, as measured by a comoving observer, is $k^{\bar{\mu}} = p^{\bar{\mu}}/p^{\bar{0}} = (1, \sin\Theta\cos\Phi, \sin\Theta\sin\Phi, \cos\Theta)$ and $k^\mu = p^\mu/p^{\bar{0}}$, where p^μ is the normalized photon four-momentum in the coordinate frame. The expressions for k^μ can be found in Appendix A of Thorne (1974) (see also Appendix C in Rueda, Ruffini & Kerr 2022). The factor $C = C(r, \Theta, \Phi)$ is the *capture function* that takes the value 1 or 0 when photons emitted at radius a r with local direction (Θ, Φ) are captured by the BH or escape to infinity, respectively. The surface

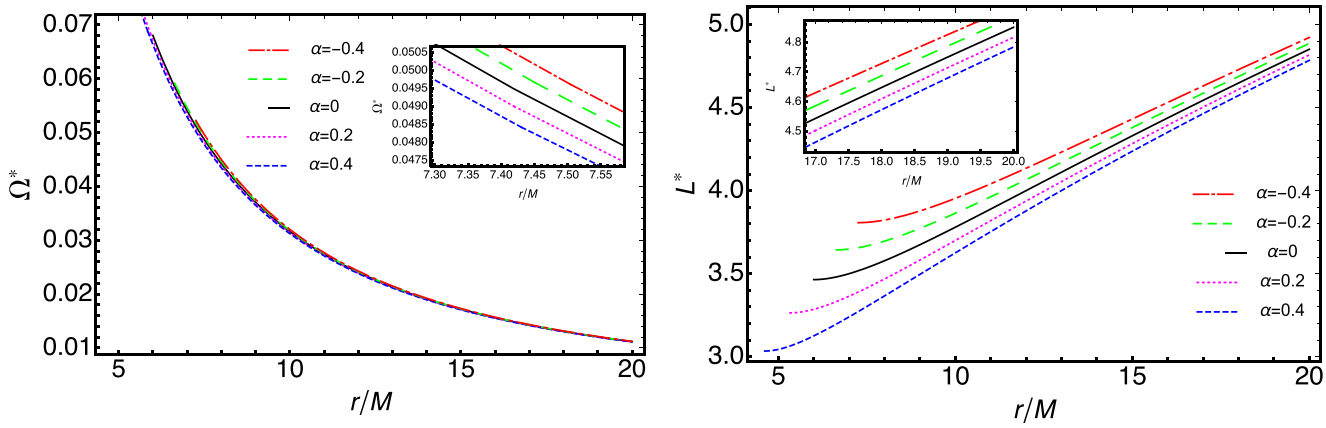

Figure B1. Left-hand panel: Angular velocity of test particles versus radial distance r in units of the BH mass, M. Right-hand panel: Angular momentum L^* of test particles versus radial distance r in units of the BH mass, M.

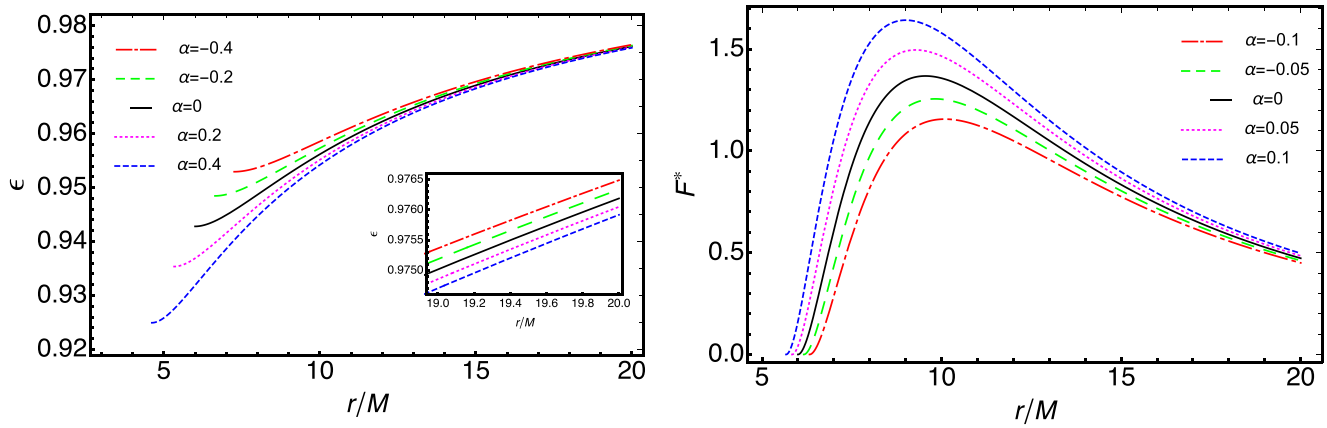

Figure B2. Left-hand panel: Energy E^* of test particles versus radial distance r in units of the BH mass, M. Right-hand panel: radiative flux $\mathcal{F}^*$ multiplied by 10^5 of the accretion disc versus radial distance r in units of the BH mass, M.

area element is $\mathrm{d}S = 2\pi r \sin\Theta\cos\Theta \mathrm{d}\Phi\mathrm{d}\Theta\mathrm{d}r$. The function $F(r)$ is the radiation flux emitted from the disc measured by the comoving observer (Novikov & Thorne 1973; Page & Thorne 1974)

$$F(r) = -\frac{\dot{m}}{4\pi\sqrt{-g}}\frac{\Omega_{,r}}{(\epsilon-\Omega l)^2}\int_{r_0}^{r}(\epsilon-\Omega l)l_{,\bar{r}}\mathrm{d}\bar{r}, \tag{B9}$$

where $\sqrt{-g} = e^{\nu+\psi+\mu} = r, \epsilon$, and l is the specific energy and angular momentum of circular geodesics of radius r in Kerr-metric (measured at infinity), and $\Omega = u^{\phi}/u^{t}$ is their angular velocity measured in the coordinate frame, being u^{μ} the fluid four-velocity Bardeen (1973). Using the change of variable $x = \sqrt{r/M}$ we can write

$$\epsilon = \frac{x^3 - 2x \pm \alpha}{x^{3/2}\sqrt{x^3 - 3x \pm 2\alpha}}, \tag{B10}$$

$$l = \pm\frac{M\left(x^4 \mp 2\alpha x + \alpha^2\right)}{x^{3/2}\sqrt{x^3 - 3x \pm 2\alpha}}, \tag{B11}$$

$$\Omega = \frac{1}{M}\frac{1}{\alpha \pm x^3}, \tag{B12}$$

where $\alpha = a/M$ is the dimensionless spin parameter. The upper/lower sign corresponds to co-rotating/counter-rotating circular orbits. Clearly, we have $\epsilon_0 = \epsilon(r_0)$ and $l_0 = l(r_0)$. The radius of the ISCO is given by Bardeen (1973)

$$r_0 = M\left[3 + Z_2 \mp \sqrt{(3-Z_1)(3+Z_1+2Z_2)}\right], \tag{B13}$$

$$Z_1 = 1 + \left(1-\alpha^2\right)^{1/3}\left[(1+\alpha)^{1/3} + (1-\alpha)^{1/3}\right], \tag{B14}$$

$$Z_2 = \sqrt{3\alpha^2 + Z_1}, \tag{B15}$$

In Fig. B1, we plot the orbital angular velocity $\Omega^* = M\Omega$ (left-hand panel) and angular momentum $L^* = l/M$ (right-hand panel) of test particles as a function of radial coordinate in the Kerr metric, for selected values of the spin parameter. Counter-rotating test particles possess larger angular velocity and momentum than co-rotating particles [for details, see Boshkayev et al. (2020, 2021)].

In Fig. B2, the energy per unit mass ϵ of test particles is shown as a function of radial coordinate (left-hand panel) and the radiative flux $F^* = 10^5 M^2 F/\dot{m}$ emitted from the accretion disc as a function of radial coordinate (right-hand panel) for different values of the spin parameter.

This paper has been typeset from a TEX/LATEX file prepared by the author.